UCRL - 72953
~~PREPRINT~~

LAWRENCE LIVERMORE LABORATORY
University of California/Livermore California

A DILATANCY MODEL FOR GRANODIORITE

J. T. Cherry
R. N. Schock

November 22, 1971

withdrawn
~~This paper was prepared for submittal to the Journal of Geophysical Research~~

A Dilatancy Model for Granodiorite

J. T. Cherry*
R. N. Schock

Lawrence Livermore Laboratory, University of California
Livermore, California 94550

A dilatancy model is described that, when used in a Lagrangian stress-wave code, qualitatively reproduces the stress-strain behavior of granodiorite subjected to triaxial stress and uniaxial strain compression. The model allows inelastic strains (voids) to progressively develop in a zone when the stress state exceeds a predetermined limit. With tension positive, the inelastic strain is assumed to be in the direction of the maximum principal stress of the zone. Numerical and experimental comparisons of triaxial compression, uniaxial strain, and Hugoniot elastic limit data for Climax stock granodiorite are presented. These comparisons indicate that the model can be used to obtain the stress-strain relations that are appropriate for other brittle rocks subjected to a variety of loading states.

Introduction

It is well known that brittle rocks subject to triaxial compression may exhibit significant volume expansion (dilatancy) prior to

*Now at Systems, Science and Software, La Jolla, California 92037.

ultimate failure. Scholz [1968] found that this dilatancy correlated with the degree of microfracturing exhibited by a specimen during a triaxial-compression test as measured by cumulative seismic events.

The availability of Lagrangian stress-strain codes such as SOC [Cherry and Petersen, 1970] and TENSOR [Cherry et al., 1970] has allowed the development of a model of dilatant microfracturing that can be tested against experimental data. These codes provide a numerical solution to the propagation of a stress wave of arbitrary amplitude through a Lagrangian grid in either one space dimension (SOC) or two space dimensions (TENSOR). The stress-strain behavior of a granodiorite* under triaxial compression is simulated numerically by incorporating the model in the TENSOR code and under uniaxial strain loading in the SOC code. A description of the model and a comparison of both simulations with experimental data is the subject of this paper.

The SOC and TENSOR Codes

In the SOC and TENSOR codes, an attempt is made to model a stress-wave loop in which a wave propagates because the strain field is altered by the presence of a stress field, with the strain field in

---

*Climax stock granodiorite from Area 15 of the Nevada Test Site. This rock is also referred to in other reports under the names Hardhat or Piledriver.

turn altering the original stress field. A schematic of one computational cycle is shown in Figure 1.

A Lagrangian coordinate system is established in the material and moves with the material. This means that the material is zoned into elements whose mass remains constant. The Eulerian equations of motion are transformed into the Lagrangian coordinate system, and the transformed equations are differenced. The difference equations provide a functional relation between the applied stress field and the acceleration of a point in the Lagrangian mesh.

When these accelerations are allowed to act over a small time increment (Δt), a new velocity field develops. The new velocities produce new displacements and the grid becomes further distorted. Strains are then derived from the grid distortion. Strain changes are related to stress changes through the equation of state appropriate for the material being simulated. The time is incremented by Δt, and the cycle is repeated with the new stresses and new zone coordinates.

The Model

Both codes require specific-volume data as a function of mean pressure as input. Figure 2 shows the measured hydrostat [Stephens and Lilley, 1970] for Climax stock granodiorite. At a given volume, the slope of this pressure-volume curve establishes the bulk modulus (k) of the material when stress deviators (i.e., shear stresses) are absent from the stress state. The curve is put directly into the codes in tabular form. The dilatancy model allows each zone to increase in volume (i.e., to move off to the right of the hydrostat) by separating the zone into a material region and a void region. The voids are assumed to develop at a prescribed shear-stress level and are presumed to be analogous to the microfractures postulated by Scholz.

Figure 3 shows the ultimate strength (Y_S) of Climax stock granodiorite as a function of $\overline{P}$ as determined from triaxial-compression tests [Heard, 1970].

In the codes, both Y and $\overline{P}$ are obtained from stress invariants [Cherry and Peterson, 1970]:

$$Y = \left(\frac{3}{4} I_{2D}\right)^{1/2}$$

and

$$\overline{P} = P - \frac{1}{2}\left(\frac{I_{3D}}{2}\right)^{1/3}$$

where I_{2D} and I_{3D} are the second and third deviatoric invariants and P is the mean stress ($-I_1/3$). For a stress state in which the intermediate principal stress is equal to either the maximum or the minimum principal stress, Y equals half the difference of and $\overline{P}$ equals half the sum of the maximum and minimum principal stresses. This interpretation of Y and $\overline{P}$ is sufficient for the results presented in this paper.

For the code calculations, it was arbitrarily assumed that dilatancy begins at half the maximum strength (lower curve Y_D in Figure 3) under triaxial compression. This assumption worked well for granodiorite. However, the onset of dilatancy may be obtained directly from the triaxial test results and therefore should be regarded as a measurable material parameter.

Y_S (and Y_D) as a function of $\overline{P}$ are accepted by the codes in tabular form. During each cycle and for each zone in the grid, the codes calculate the Y from the stress in each zone. We call this $\tilde{Y}$. When the $\tilde{Y}$ for a given zone exceeds Y_D, an additional strain (Δe_{AA}) is allowed to develop in the direction of the zone's maximum principal stress, with tension positive. This strain is assumed to take the form of a small tension crack that opens in the zone. The crack is oriented normal to the maximum principal stress. Therefore, if $\tilde{T}_{AA}$ is a zone's maximum principal stress, and if

$$Y_D < \tilde{Y} < Y_S \tag{1}$$

then

$$P = \tilde{P} + k\Delta e_{AA} \tag{2}$$

$$T_A = \tilde{T}_A - \frac{4}{3}\mu\Delta e_{AA}$$

$$T_B = \tilde{T}_B + \frac{2}{3}\mu\Delta e_{AA}$$

$$T_C = \tilde{T}_C + \frac{2}{3}\mu\Delta e_{AA}$$

where $\tilde{P}$ is the mean stress associated with the zone and $\tilde{T}_A$, $\tilde{T}_B$, and $\tilde{T}_C$ are the stress deviators in the principal coordinate system. In this system, $\tilde{T}_{AA}$, $\tilde{T}_{BB}$, and $\tilde{T}_{CC}$ are the principal stresses and

$$\tilde{P} = -\frac{1}{3}(\tilde{T}_{AA} + \tilde{T}_{BB} + \tilde{T}_{CC}) \qquad (3)$$

$$\tilde{T}_A = \tilde{P} + \tilde{T}_{AA}$$

$$\tilde{T}_B = \tilde{P} + \tilde{T}_{BB}$$

$$\tilde{T}_C = \tilde{P} + \tilde{T}_{CC}$$

Also,

$$T_A + T_B + T_C = \tilde{T}_A + \tilde{T}_B + \tilde{T}_C = 0 \qquad (4)$$

The inelastic strain (Δe_{AA}) is added to both the mean stress and the deviatoric stress components associated with the expansion of the crack as shown in (2). k and μ are the bulk and shear moduli of the intrinsic solid. When Δe_{AA} is determined, the adjusted stress components (P, T_A, T_B and T_C) can be found for the zone and used to drive the grid for the next cycle.

Since

$$Y^2 = \frac{3}{2}\left(T_A^2 + T_B^2 + T_C^2\right) \tag{5}$$

$$\tilde{Y}^2 = \frac{3}{2}\left(\tilde{T}_A^2 + \tilde{T}_B^2 + \tilde{T}_C^2\right)$$

then

$$\frac{2}{3}\mu\Delta e_{AA} = \frac{1}{2}\left[\tilde{T}_A - \sqrt{\tilde{T}_A^2 - \frac{16}{9}\left(\tilde{Y}^2 - Y^2\right)}\right] \tag{6}$$

where

$$Y^2 = \tilde{Y}^2 - \left\{\tilde{Y}^2 - (Y^n)^2\right\}(ab)^2;\ \tilde{Y} > Y^n \tag{7}$$

$$= \tilde{Y}^2;\ \tilde{Y} < Y^n$$

$$a = \frac{\tilde{Y} - Y_D}{Y_S - Y_D}$$

$$b = \left(\frac{dY}{dP}\right)_D + a\left[\left(\frac{dY}{dP}\right)_S - \left(\frac{dY}{dP}\right)_D\right]$$

$$0 < a < 1$$

$$0 < b < 1$$

and Y^n represents the Y from the previous cycle.

Equations 6 and 7 are the basic equations used in the codes to find Δe_{AA}. Equation 6 is obtained by substituting the adjusted deviatoric stress relations of (2) into (5) and solving for Δe_{AA}. Equation 7 gives the rule used in the codes to obtain the adjusted value of Y^2. Once the formulization of (1) through (6) is adopted so that the inelastic strain is allowed to develop in the direction of the maximum principal stress, almost any flow rule that allows Y^2 to be less than $\bar{Y}^2$ will produce dilatancy in the calculations. The problem is to make the flow rule general enough so that it represents a variety of experimental tests.

The a factor in (7) ensures that maximum adjustment occurs as $\bar{Y}$ approaches the material strength (Y_S). This is consistent with the observation that dilatancy increases with increasing deviatoric stress at a fixed confining pressure [Brace, Paulding, and Scholz, 1966]. The failure envelope is intersected when a = 1. The b factor in (7) allows the adjustment to vary directly with the slopes of the Y_S and Y_D curves as the latter vary with $\bar{P}$. In other words, the amount of dilatancy is presumed to be a function of $\bar{P}$ [Schock and Duba, to be published; Schock, Heard, and Stephens, 1973]. If the Y_S and Y_D curves do not vary with $\bar{P}$, the material is considered to be yielding plastically and dilatancy is precluded. This implies that dilatancy is related to brittle failure.

Equation 7 has worked adequately in simulating test results with Climax stock granodiorite. While this equation is a necessary part of the dilatancy model, it does not represent a general flow rule for all brittle rocks. The portion of the model that is most important and that is least likely to change is given by (1) through (6). Equation 7 only controls the amount of dilatancy that is allowed to develop at a given stress state.

A deficiency of the dilatancy model is that it is not able to simulate a material that both plastically yields and dilates simultaneously. This is because of the fact that the entire adjustment on the second deviatoric invariant, given by (7), is folded into the expression for Δe_{AA} in (6). This deficiency could be removed by allowing only a portion of the flow rule to produce a contribution to Δe_{AA}. The final deviatoric stress components could then be obtained by simple scaling.

Throughout the development of the model, no attempt was made to quantitatively reproduce experimental data with a code calculation. This was partly due to sample variability and partly because some of the calculations were completed before test results were available. The μ used in the calculations was 250 kbar and was determined from the low-pressure bulk modulus (k = 487 kbar) [Stephens and Lilley, 1970], the material density (2.67 g/cm^3), and the elastic compressional velocity (5.54 km/sec) [Butkovich, 1965].* This equation of state was used as input to the codes

*R. N. Schock and H. Louis, Lawrence Livermore Laboratory, later measured a velocity of 5.70 km/sec in a 3-cm-long sample of Climax stock granodiorite under a confining pressure of 1 bar. This is higher than the in-situ value given above, and it probably represents the absence of any effect of large cracks and joints present in the intrusive. This interpretation is reinforced by the values of μ that are measured in the experiments described below and that are larger than the value derived above.

for all of the simulated tests. The experimental data were collected in an apparatus that is designed to apply a hydrostatic end load to a cylindrical sample while under confining pressure [Seigel and Haba, to be published]. This eliminates the end effects commonly associated with loading utilizing a solid piston and results in more accurate data.

Triaxial Compression

Figure 4 shows the Lagrangian grid used in the TENSOR code to simulate the triaxial-compression test. A reflecting boundary condition that is available in the code reflects the grid across the two lines marked "R." This feature allows the grid to represent a cylinder having a diameter of 3 cm and a length of 6 cm. A constant velocity of 3 cm/sec was applied along the top surface, resulting in an initial strain rate of 1 sec^{-1}. While this strain rate is orders of magnitude larger than that used in the laboratory experiments, it is still low enough to obtain a uniform stress distribution throughout the grid in the computer calculation. The boundary marked "F" was a free surface along which a constant pressure (the confining pressure) is applied.

The model was used to simulate two triaxial-compression experiments, one unconfined and the other at a confining pressure of 0.5 kbar. The displacement field (S_r, S_z) in the region marked "strain" in Figure 4 was monitored at selected times. This displacement field provided enough information to calculate both the axial strain ($e_{zz} = \Delta S_z/\Delta z$) and the radial strain ($e_{\theta\theta} = S_r/r$). The average axial stress ($\bar{T}_{zz}$) was also calculated along the top and bottom of the grid at the same time as the surface displacements were monitored. The axial stress at the top and bottom of the grid differed by less than 0.1% during the calculations, indicating that the 1 sec^{-1} strain rate is still low enough to give a uniform stress distribution over the entire grid.

The TENSOR-calculated stress-strain curves can be compared with the corresponding measurements obtained during the equivalent laboratory experiments. Figure 5 shows the measured and calculated axial stress versus the volumetric strain corresponding to unconfined compression. The difference between the curves is because an average granodiorite strength equal to 1.6 kbar of axial stress for unconfined compression was used in the code, whereas the sample strength obtained from the experiment was 2.2 kbar. The slight difference in the initial slopes of the curves is because the measured effective values of μ and k are slightly different from those used as input to the code. The measured value of μ in this experiment was 265 kbar. The increased level of failure above that shown in Figure 3 may be because of the absence of spurious shear stresses at the ends of the sample that are caused by a compliance mismatch between the sample ends and a solid piston. The failure level obtained here is reproducible to within 10%. The data of Heard [1970] were all obtained using a solid piston. In the code, shear failure occurred at a calculated volumetric strain $(-e_{zz} - 2e_{\phi\phi})$ of -1.2×10^{-3}, well off the horizontal scale. The real volumetric strain $((V_0 - V)/V)$ of the zone at failure was -2.8×10^{-4}.* The

*This strain is obtained in the code by accumulating volume changes from cycle to cycle. The zone referred to is the element in the lower right-hand corner of Figure 4 bounded by the "R" and "F" surfaces.

difference between the calculated and the accumulated volumetric strains is significant. It occurs because the radial strain is no longer equal to the tangential strain when the volumetric strain associated with dilation is large, and because $+e_{zz} - 2e_{\phi\phi}$ is therefore no longer a good approximation of the volumetric strain. The measured experimental volumetric strain at failure was somewhat greater than -3.4×10^{-3}, presumably owing to the greater strength of the sample.

Figure 6 compares the measured and calculated axial stress versus the axial strain (e_{zz}) for unconfined compression. Both curves exhibit an increase in their slopes prior to failure. Figure 7 compares the measured and calculated axial stress versus the tangential strain ($e_{\phi\phi}$). The model drastically changes this strain component during the dilatancy adjustment because the stress component in the tangential direction is a maximum principal stress.

Figure 8 shows the measured and calculated axial stress versus the volumetric strain corresponding to triaxial compression at a confining pressure of 0.5 kbar. The slight difference in the origins of the curves represents the experimental hydrostatic compression to 0.5 kbar being slightly greater than the table of input values for k as taken from Figure 2. Agreement in this case is quite good since the average strength used in the TENSOR code is close to the sample strength obtained from the experimen[t]. At higher confining pressures, better agreement would be expected between data obtained by solid-piston and fluid loading because the shear stresses that arise from a compliance mismatch with the solid piston would be smaller with respect to the overall stress level than when there is no confining pressure. In this case, failure occurred at a calculated volumetric strain of 2.5×10^{-3}, whereas the real volumetric strain of the zone at failure was 2.7×10^{-3}. The inelastic volumetric strain has decreased by a factor of 2 compared to the value obtained for unconfined compression. The measured experimental volumetric strain at failure was slightly more than 2.5×10^{-3}.

Uniaxial Strain and the Hugoniot Elastic Limit

Both uniaxial-strain and Hugoniot data have been simulated with the dilatancy model in the SOC code. Figure 9 shows Hugoniot data [Petersen, 1969] for Climax stock granodiorite. Hugoniot data for Westerly granite are shown above 200 kbar, where they overlap the granodiorite data, in order to show the likely loading data for granodiorite at higher pressures. The Rayleigh line through the Hugoniot elastic limit (HEL) intersects the Hugoniot at about 325 kbar. For shock states below 325 kbar, the first arrival is the HEL.

Figure 10 shows the SOC calculation for a final shock state of 200 kbar in Climax stock granodiorite. The HEL is propagating with a velocity of about 6 m/msec and has an amplitude of 35 kbar. In Figure 11, the experimental HEL data are compared with the HEL point calculated by SOC. The calculated point falls within the range of the experimental data.

Figures 12 and 13 compare the measured and calculated uniaxial-strain data on Climax stock granodiorite. The slight offset between the calculated and experimental curves in Figure 13 is caused by the slight difference between the effective Poisson's ratio measured in the sample and the ratio used in the equation of state in the code. The effective Poisson's ratio determines the slope of a loading path in uniaxial-strain loading in Y-$\overline{P}$ space.

Conclusions

The dilatant behavior of brittle rocks prior to ultimate failure is easily modeled by assuming that an inelastic strain develops in the direction of the maximum principal stress. The size of this strain depends on an assumed flow rule. The flow rule for granodiorite depends on how the strength and dilatancy-onset values put into the SOC and TENSOR codes vary with $\overline{P}$, as well as on the stress state in the zone. The dilatancy model described in this paper has been used to simulate the results of a number of rock-mechanics experiments, including triaxial compression, uniaxial strain, and plane-shock loading (Hugoniot).

Rock-mechanics tests are being used to model and to attempt to control earthquakes. The experimental results that have been used so far are the stress drop at shear failure and the strength reduction from fluid saturation. In terms of earthquake prediction, dilatancy may be a significant tool once its effect on the regional strain field is understood. Since the model presented here has been formulated in terms of strain adjustment, it is possible that it may be useful, in conjunction with a suitable numerical technique, in obtaining an understanding of this effect.

Acknowledgments. We gratefully acknowledge the programming and software support of V. J. Kransky, F. L. Petersen, and J. G. Shaw and discussions with A. G. Duba and D. R. Stephens. This work was performed under the auspices of the U.S. Atomic Energy Commission.

References

Brace, W. F., B. W. Paulding Jr., and C. Scholz, Dilatancy in the fracture of crystalline rocks, J. Geophys. Res., 71, 3939-3953, 1966.

Butkovich, T. R., Calculation of the shock wave from an underground nuclear explosion in granite, J. Geophys. Res., 70, 885-892, 1965.

Cherry, J. T., and F. L. Petersen, Numerical simulation of stress wave propagation from underground nuclear explosions, in Proc. Symp. Eng. Nucl. Explosives (CONF-700101), Vol. 1, pp. 142-220, American Nuclear Society and U.S. Atomic Energy Commission, 1970.

Cherry, J. T., S. Sack, G. Maenchen, and V. Kransky, Two-dimensional stress-induced adiabatic flow, Rep. UCRL-50987, Lawrence Livermore Laboratory, Livermore, California, 1970.

Heard, H. C., The influence of environment on the inelastic behavior of rocks, in Proc. Symp. Eng. Nucl. Explosives (CONF-700101), Vol. 1, pp. 127-141, American Nuclear Society and U.S. Atomic Energy Commission, 1970.

Petersen, C. F., Shock wave studies of selected rocks, Ph. D. dissertation, Stanford University, Palo Alto, California, 1969.

Schock, R. N., and A. Duba, Quasi-static deformation of solids with pressure (to be published in J. Appl. Phys.).

Schock, R. N., H. C. Heard, and D. R. Stephens, Mechanical properties of graywacke sandstone and granodiorite, Trans. Am. Geophys. Union, 52, 345-346, 1971.

Scholz, C. H., Microfracturing and the inelastic deformation of rock in compression, J. Geophys. Res., 73, 1417-1432, 1968.

Stephens, D. R., and E. M. Lilley, Loading-unloading pressure-volume curves for rocks, in Proc. Symp. Eng. Nucl. Explosives (CONF-700101), Vol. 1, pp. 89-109, American Nuclear Society and U.S. Atomic Energy Commission, 1970.

FIGURE CAPTIONS

Fig. 1. Cycle of interactions treated in calculating stress-wave propagation.

Fig. 2. Hydrostatic volume compression of Climax stock granodiorite [Stephens and Lilley, 1970].

Fig. 3. Strength of Climax stock granodiorite as a function of confining pressure [Heard, 1970] and the assumed onset of dilatancy.

Fig. 4. Lagrangian grid used in the TENSOR code to simulate triaxial compression.

Fig. 5. Measured and calculated volumetric strain as a function of axial stress in Climax stock granodiorite under a confining pressure of 1 bar.

Fig. 6. Measured and calculated axial strain as a function of axial stress in Climax stock granodiorite under a confining pressure of 1 bar.

Fig. 7. Measured and calculated tangential strain as a function of axial stress in Climax stock granodiorite under a confining pressure of 1 bar.

Fig. 8. Measured and calculated volumetric strain as a function of axial stress in Climax stock granodiorite under a confining pressure of 0.5 kbar.

Fig. 9. Hugoniot and compression data for Climax stock granodiorite and Westerly granite.

Fig. 10. Calculated normal stress as a function of distance in Climax stock granodiorite, showing the Hugoniot elastic limit for a final shock state of 200 kbar ($t = 3.5$ μsec).

Fig. 11. Measured and calculated Hugoniot-elastic-limit data for Climax stock granodiorite.

Fig. 12. Measured and calculated volumetric strain as a function of axial stress in Climax stock granodiorite under uniaxial-strain loading.

Fig. 13. Measured and calculated stress states in Climax stock granodiorite under uniaxial-strain loading.

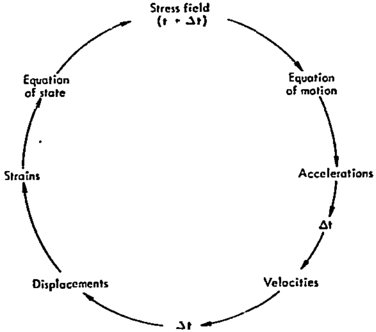
Stress field
(t + Δt)
Equation
of motion
Accelerations
Δt
Velocities
Δt
Displacements
Strains
Equation
of state

Cherry - Fig. 1

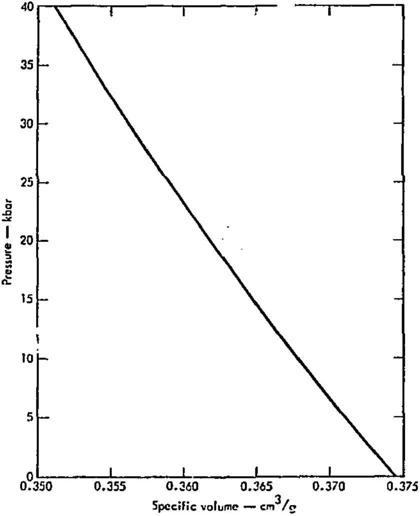

40
35
30
25
20
15
10
5
0
Pressure — kbar
0.350
0.355
0.360
0.365
0.370
0.375
Specific volume — cm^3/g

Cherry - Fig. 2

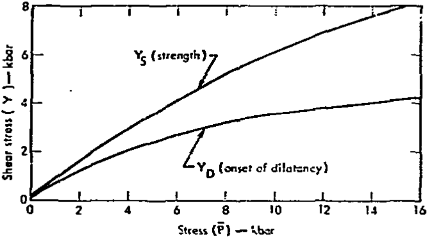

Shear stress (Y)— kbar
Stress ($\bar{P}$) — kbar
Y_S (strength)
Y_D (onset of dilatancy)
0
2
4
6
8
10
12
14
16

Cherry - Fig. 3

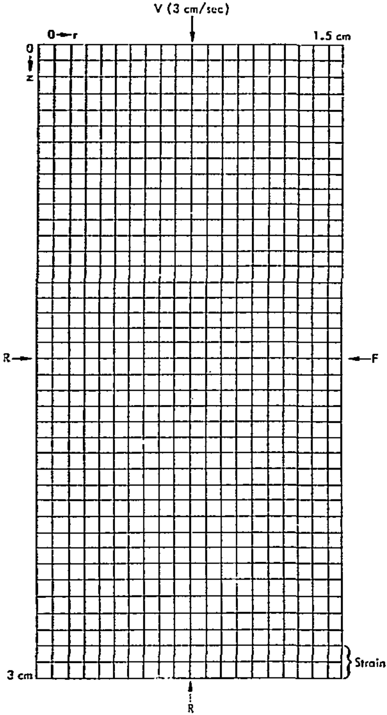

Cherry - Fig. 4

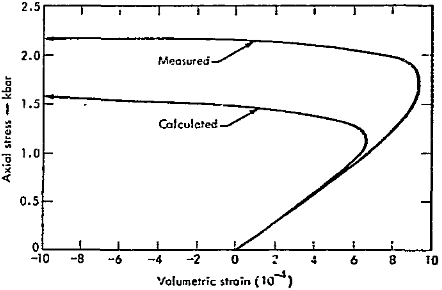

2.5
2.0
1.5
1.0
0.5
0
Axial stress — kbar
Measured
Calculated
−10
−8
−6
−4
−2
0
2
4
6
8
10
Volumetric strain (10^{-4})

Cherry - Fig.

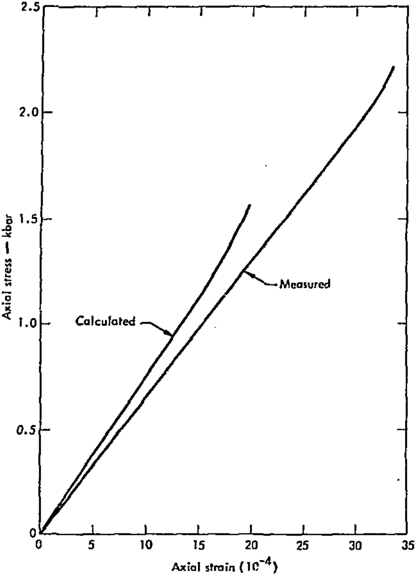
2.5
2.0
1.5
1.0
0.5
0
Axial stress — kbar
Calculated
Measured
0
5
10
15
20
25
30
35
Axial strain (10^{-4})

Cherry - Fig. 6

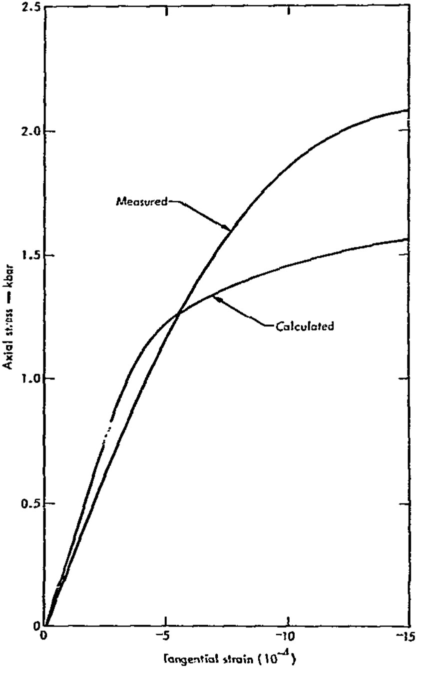

2.5
2.0
1.5
1.0
0.5
0
Axial stress — kbar
Measured
Calculated
0
-5
-10
-15
Tangential strain (10^{-4})

Cherry - Fig. 7

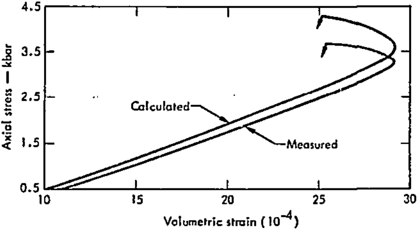
4.5
3.5
2.5
1.5
0.5
Axial stress — kbar
Calculated
Measured
10
15
20
25
30
Volumetric strain (10^{-4})

Cherry - Fig. 8

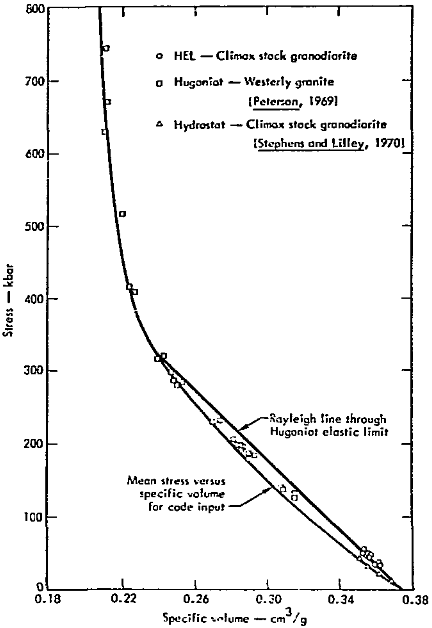

HEL — Climax stock granodiorite
Hugoniot — Westerly granite
[Peterson, 1969]
Hydrostat — Climax stock granodiorite
[Stephens and Lilley, 1970]
Rayleigh line through
Hugoniot elastic limit
Mean stress versus
specific volume
for code input
Stress — kbar
800
700
600
500
400
300
200
100
0
0.18
0.22
0.26
0.30
0.34
0.38
Specific volume — cm^3/g

Cherry - Fig.

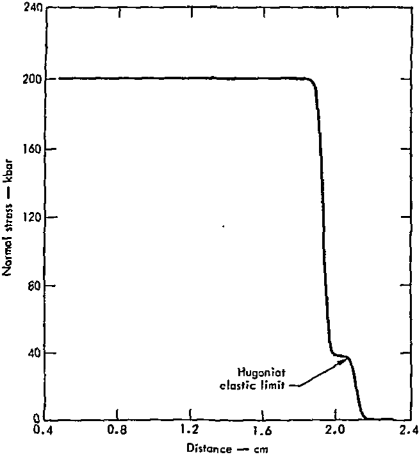

Cherry - Fig. 10

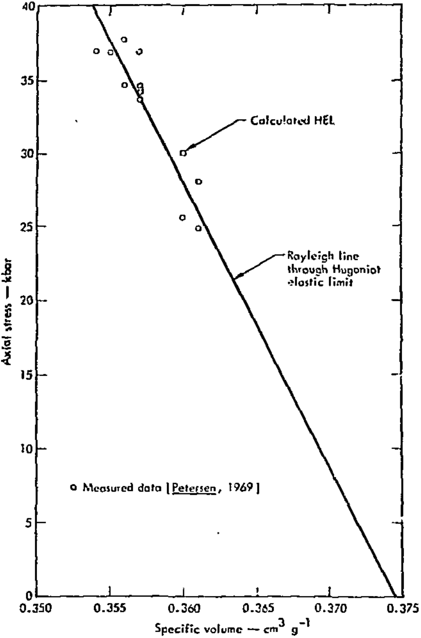

Cherry - Fig. 11

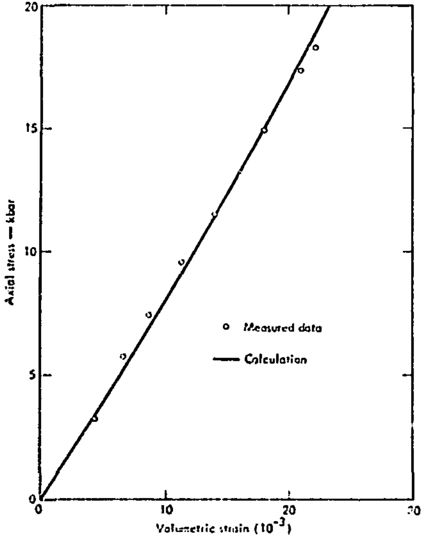

Cherry • Fig. 12

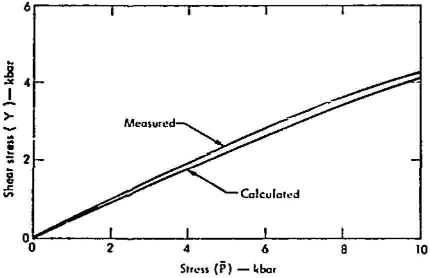

Cherry - Fig. 13